

Terahertz emission driven by two-color laser pulses at various frequency ratiosW.-M. Wang,^{1,2,5,*} Z.-M. Sheng,^{3,4,5} Y.-T. Li,^{1,5,6} Y. Zhang,² and J. Zhang^{3,5}¹*Beijing National Laboratory for Condensed Matter Physics, Institute of Physics, CAS, Beijing 100190, China*²*Beijing Advanced Innovation Center for Imaging Technology and Key Laboratory of Terahertz Optoelectronics (MoE), Department of Physics, Capital Normal University, Beijing 100048, China*³*Key Laboratory for Laser Plasmas (MoE) and Department of Physics and Astronomy, Shanghai Jiao Tong University, Shanghai 200240, China*⁴*SUPA, Department of Physics, University of Strathclyde, Glasgow G4 0NG, United Kingdom*⁵*IFSA Collaborative Innovation Center, Shanghai Jiao Tong University, Shanghai 200240, China*⁶*School of Physical Sciences, University of Chinese Academy of Sciences, Beijing 100049, China*

(Received 14 April 2017; published 21 August 2017)

We present a simulation study of terahertz radiation from a gas driven by two-color laser pulses in a broad range of frequency ratios ω_1/ω_0 . Our particle-in-cell simulation results show that there are three series with $\omega_1/\omega_0 = 2n, n + 1/2, n \pm 1/3$ (n is a positive integer) for high-efficiency and stable radiation generation. The radiation strength basically decreases with the increasing ω_1 and scales linearly with the laser wavelength. These rules are broken when $\omega_1/\omega_0 < 1$ and much stronger radiation may be generated at any ω_1/ω_0 . These results can be explained with a model based on gas ionization by two linear-superposition laser fields, rather than a multiwave mixing model.

DOI: [10.1103/PhysRevA.96.023844](https://doi.org/10.1103/PhysRevA.96.023844)**I. INTRODUCTION**

Strong terahertz (THz) waves have broad applications in physics [1–4], biology [5], and medicine [6]. A large number of studies have shown that interactions of intense fs laser pulses with plasmas can provide powerful table-top THz sources with tunable parameters. Near mJ level of THz radiation with large divergence and a band from 0.1 THz to 100 THz [7–12] has been observed from solid targets interacted by relativistic intense laser pulses. Nearly linearly polarized, single-cycle, MV/cm-scale THz radiation with good directionality [13–27] has been generated from a gas irradiated by weakly relativistic intense laser pulses, via the well-known two-color laser scheme in which a fundamental laser pulse is mixed with a second pulse at the second harmonic [13]. With circularly polarized or elliptically polarized driving laser pulses [28–30], the radiation can become elliptically polarized. When an external magnetic field is imposed in the two-color scheme with linearly polarized laser pulses, the radiation can be narrow-band, circularly polarized [31].

To further achieve more powerful THz radiation, a few schemes were proposed by increasing the laser wavelength. In 2011, a midinfrared laser scheme was proposed to significantly enhance the radiation strengths [32], because the ionization symmetry in a laser cycle can be broken more strongly with a longer wavelength laser pulse. The subsequent experiments [33,34] showed that midinfrared laser pulses are more favorable for THz generation than conventional 0.8 μm wavelength pulses. In particular, a strong dependence of THz generation on the laser wavelength in the two-color laser scheme was found [34,35] and 4.4 MV/cm THz radiation was generated in experiments with a 1.8 μm wavelength pulse and its second harmonic pulse [34].

A few recent works showed that the two-color laser scheme can be extended. In 2013, a model based on linear superposi-

tion of two laser fields predicted [36] that as long as the frequency ratio ω_1/ω_0 of the two laser pulses is $2n$ (n is a positive integer), THz radiation can be generated, which was verified by particle-in-cell (PIC) simulations. In 2016, Kostin *et al.* [37] performed detailed calculations with ω_1/ω_0 from 0.4 to 3 and found THz radiation can be generated when ω_1/ω_0 are 2/3, 3/2, etc. They proposed a multiwave mixing theory to well explain their calculation results. In addition, Gonzalez de Alaiza Martinez *et al.* [38] proposed that if the two-frequency pulses are extended to multiple-frequency pulses with fixed phases and strengths for each pulse (it is a sawtooth wave in the limit case), the THz strength can be significantly increased.

In this paper, we further study the two-color laser scheme with broader frequency ratios to generate THz radiation. When the frequency ratio ω_1/ω_0 is limited within 0.4 and 3, our PIC simulation results agree with the calculation results in Ref. [37], which can be described by the multiwave mixing theory. However, when the region of ω_1/ω_0 is extended to be below 0.4, the predictions by the multiwave mixing theory contradict with our PIC results. Contrary to the predictions [37], the THz radiation could be generated at any $\omega_1/\omega_0 = a : b$ (a and b are natural), even if $a + b$ is even, the upper limit of $a + b$ for the THz generation does not depend on the laser intensity, and the THz generation is not necessarily weakened with the growing $a + b$, e.g., the radiation with $\omega_1/\omega_0 = 3/10$ can be stronger than the one with $\omega_1/\omega_0 = 3/2$. These results can be explained by gas ionization by two linear-superposition laser fields, suggesting that the multiwave mixing theory might not reflect the physical insights.

We find that when ω_1/ω_0 is $2n, n + 1/2, n \pm 1/3$ (n is a positive integer), the THz generation is highly efficient and stable against the changing laser duration and intensity, where the $2n$ series has the best performance. The THz strength basically decreases with the increasing n and scales linearly with the laser wavelength in the tunneling ionization regime. With this linear wavelength scaling, one can link the THz generation in the two cases between $\omega_1/\omega_0 = 2/3$ and $3/2$, or

*weiminwang1@126.com

between $\omega_1/\omega_0 = 1/2$ and 2, or between $\omega_1/\omega_0 = 1/4$ and 4, etc. These simulation results are explained by a model based on gas ionization by two linear-superposition laser fields.

II. THZ GENERATION WITH VARIOUS FREQUENCY RATIOS

A. Setup of PIC simulation

We first present results of PIC simulations with the two-dimensional (2D) KLAPS code [39] and then explain the PIC results by a theoretic model. In the PIC code [39], the field ionization of gases is included and the full Maxwell equations are used to calculate electromagnetic-field generation and propagation. Therefore, it can self-consistently calculate the plasma production and net current formation via ionization by the incident laser pulses, dynamics of the net current in the plasma, and THz radiation generation. Note that the dispersion and absorption of electromagnetic waves in formed plasma is taken into account, but the dispersion and absorption in a gas is not included, which could be ignored in a near-field case or a short distance of propagation. In the current study, the laser wavelength or cycle needs to be resolved since the THz generation depends on the relative phase between the two-color pulses. Thus it is difficult to compute a long distance of propagation (e.g., millimeter and centimeter scales) of laser and THz waves by PIC simulation. A (3 + 1)-dimensional simulation approach proposed by Babushkin *et al.* [40,41] can effectively calculate a long distance of propagation, based on a unidirectional pulse propagation equation, which can obtain far-field THz emission. On the other hand, the PIC approach is suitable to calculate the near-field THz radiation generation, which determines the main properties (frequency, waveform, strength, polarization, etc.) of far-field THz radiation observed in experiments, since the final far-field radiation is composed of many near-field sources [27,41]. Hence the PIC simulations can self-consistently estimate THz generation by two-color laser pulses at various frequency ratios. Note that in Ref. [37] the gas ionization is calculated, but the THz generation is not included.

In our PIC simulations, the frequency ω_0 of the first laser pulse is fixed with the wavelength $\lambda_0 = 0.8 \mu\text{m}$ (or the period $\tau_0 = 2.667 \text{ fs}$) and the second laser frequency ω_1 is changed in the range from $0.1\omega_0$ to $20\omega_0$. The two pulses propagate along the $+x$ direction with linear polarization along the y direction. They have the same spot radius $r_0 = 100 \mu\text{m}$, duration 50 fs in full width at half maximum (FWHM), and peak intensity $I_0 = I_1 = 10^{14} \text{ W/cm}^2$ (or peak strengths 274 MV/cm), as used in Ref. [37]. The total laser energy is 1.86 mJ. The laser electric fields are taken as $\mathbf{E} = \vec{e}_y [a_0 \sin(\omega_0 \psi) + a_1 \sin(\omega_1 \psi + \theta_1)] \exp(-y^2/r_0^2) f(\psi)$, where $\psi = t - x/c$, $f(\psi)$ is the Gaussian envelope profile of the laser pulses, and the relative phase θ_1 of the two pulses is zero (note that at $\theta_1 = 0$ the strongest radiation can be generated with $\omega_1/\omega_0 = 2n, n + 1/2, n \pm 1/3$ according to our simulation results). A hydrogen gas slab is taken with a length $300 \mu\text{m}$ and a uniform density $4.88 \times 10^{16} \text{ cm}^{-3}$ (the corresponding plasma frequency $\omega_p/2\pi = 2 \text{ THz}$ after the complete ionization [36]). The resolutions along the x and y directions are $0.01\lambda_0$ and $0.1\lambda_0$, respectively. In the gas region, four simulation particles per cell are adopted to denote gas atoms. In all the simulations, the gas parameters and the laser relative phase are kept unchanged. In Fig. 4 and Table I

we take the standard parameters mentioned above. Besides ω_1 , only one laser parameter is changed as addressed in figure legends: we used different laser durations in Fig. 1, different laser intensities in Figs. 2 and 3, and different ω_0 in Fig. 5.

Note that we do not observe THz generation above 5 kV/cm when ω_1 is taken as $12\text{--}20\omega_0$. One can expect no THz generation with a higher value of ω_1 . For the case with $\omega_1 < 0.1\omega_0$, the pulse of 50 fs has the effective cycle number below 2. Therefore, the frequency ratio of 0.1–20 taken in our simulations should cover the whole range possibly adopted in laboratories currently.

B. PIC simulation results

Figure 1(a) displays absolute values of the THz radiation strengths observed in the left vacuum $5\lambda_0$ away from the vacuum-gas boundary. The PIC simulation results in the range of ω_1/ω_0 from 0.4 to 3 are in agreement with the results by calculating the net current generation in Ref. [37], in which the investigation is limited in this frequency range (note that the THz strength is proportional to the net current strength [19,42]). Peaks of the THz strengths appear at $\omega_1/\omega_0 = 1/2, 2/3, 4/3, 3/2, 2, 5/2$ (strength signs can be observed in Fig. 2 below), as given in Ref. [37]. As ω_1/ω_0 is reduced from 0.4 to 0.1, some new peaks arise with higher strengths than the peaks at $\omega_1/\omega_0 > 0.4$, as shown more clearly in Fig. 1(b). In particular, the strengths at $\omega_1/\omega_0 = 1/4, 1/8, 1/9, 1/10$ exceed the strength 0.17 MV/cm at $\omega_1/\omega_0 = 2$ (the original two-color scheme [13]). This result contradicts with the multiwave mixing theory proposed in Ref. [37], which drew the conclusions as follows: to generate THz radiations, $a + b$ should be an odd integer ($\omega_1/\omega_0 = a : b$, $a : b$ is irreducible, and a and b are natural) and the radiation is weakened with the increasing $a + b$. These conclusions can summarize the results with ω_1/ω_0 between 0.4 and 3. However, they are broken when ω_1/ω_0 is lower than 0.4. Strong THz radiations can be generated even if $a + b$ is even, e.g., $\omega_1/\omega_0 = 1/9$.

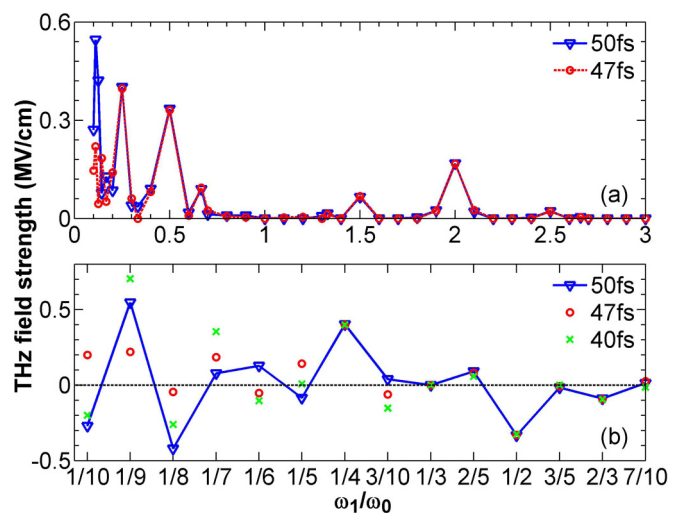


FIG. 1. THz field strength as a function of the two-color laser frequency ratio ω_1/ω_0 , where different curves correspond to different laser durations. (a) The absolute values of the THz strengths. To clearly show the strengths at low ω_1/ω_0 , a limited range of ω_1/ω_0 is taken in (b).

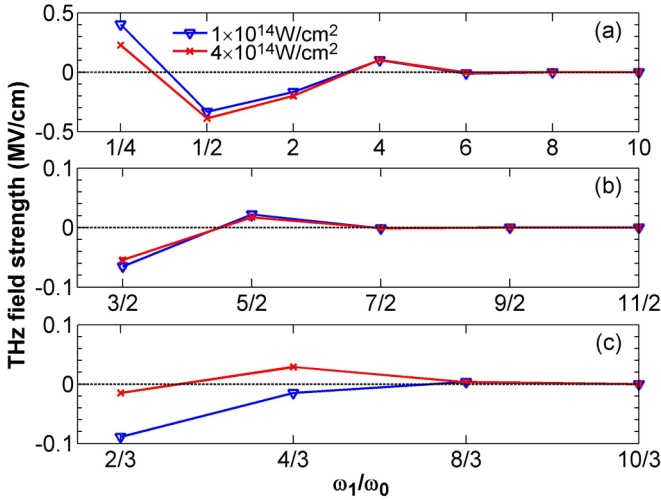


FIG. 2. THz field strength as a function of the two-color laser frequency ratio, where the two curves in each plot correspond to laser intensities of 10^{14} W/cm 2 and 4×10^{14} W/cm 2 , respectively.

The strength with larger $a + b$ is not necessarily lower, e.g., comparing the result at $\omega_1/\omega_0 = 2/3$ with the ones at $\omega_1/\omega_0 = 1/9$ or $1/6$, etc.

One of the most important conclusions given by the multiwave mixing theory [37] is that $a + b$ should be less than m_0 for the THz generation and m_0 is determined by the laser intensity, e.g., $m_0 = 11$ for $I_0 = 10^{14}$ W/cm 2 [37]. This does not agree with the results shown in Fig. 1(b) that the THz radiations can be generated at $\omega_1/\omega_0 = 1/10, 3/10$ with $a + b \geq 11$. Furthermore, if the laser intensity is enhanced, m_0 should be greater than 11 according to the multiwave mixing theory. However, when we increase the laser intensity from $I_0 = 10^{14}$ W/cm 2 to 4×10^{14} W/cm 2 (also 2×10^{14} W/cm 2), we do not observe THz generation at any new point of ω_1/ω_0 with $a + b \geq 11$, as shown in Fig. 2. In this figure we only

illustrate the results with ω_1/ω_0 at $2n$, $n + \frac{1}{2}$, $n \pm \frac{1}{3}$ (n is a positive integer), at which the THz generation has high efficiency and good stability as will be addressed below. All in all, our simulations show that there is not a cutoff of $a + b$ dependent of laser intensity, required for the THz generation.

In addition, one can see in Fig. 1 that the THz generation is significantly affected by laser duration. In this figure, we slightly change the laser duration and observe sharp varieties in the THz strengths when $\omega_1/\omega_0 < 1/3$. Even the signs of the THz strengths is reversed at some ω_1/ω_0 values, when the laser duration is changed from 50 fs to 47 fs. When $\omega_1/\omega_0 > 1/3$, the THz generation slightly changes with the laser duration. In our additional simulations, we take the laser duration to 25 fs, change the duration around this value, and find the THz strength significantly changes when $\omega_1/\omega_0 < 0.6$. Once more, this cannot be explained by the multiwave mixing theory [37].

III. EXPLANATIONS BY GAS IONIZATION OF TWO LINEAR-SUPERPOSITION LASER FIELDS

From the simulation results above, one can see that although the multiwave mixing theory [37] can summarize most results of THz generation with ω_1/ω_0 within 0.4 and 3, it is not consistent with the results with lower ω_1/ω_0 . In the following, we will explain all the results through gas ionization by two linear-superposition laser fields.

We first explain why stronger THz radiation can be generated with the lower ω_1/ω_0 , in particular $\omega_1/\omega_0 = 1/9, 1/7, 1/5$ with which the radiation should not have been generated. In Figs. 3(a)–3(e) we plot the number distribution of electrons created via ionization versus the laser-pulse envelope position. In Fig. 3(a) with $\omega_1/\omega_0 = 2$ there are two ionization points in each cycle of the ω_0 laser pulse [36] and tens of ionization points in total can be observed. In Fig. 3(e) with $\omega_1/\omega_0 = 1/9$, there are six ionization points in each ω_1 laser cycle $\tau_1 = 9\tau_0$ (e.g., a cycle from $t - x/c = 10\tau_0$ to $19\tau_0$) and the total ionization points are less. Note that the total laser field and

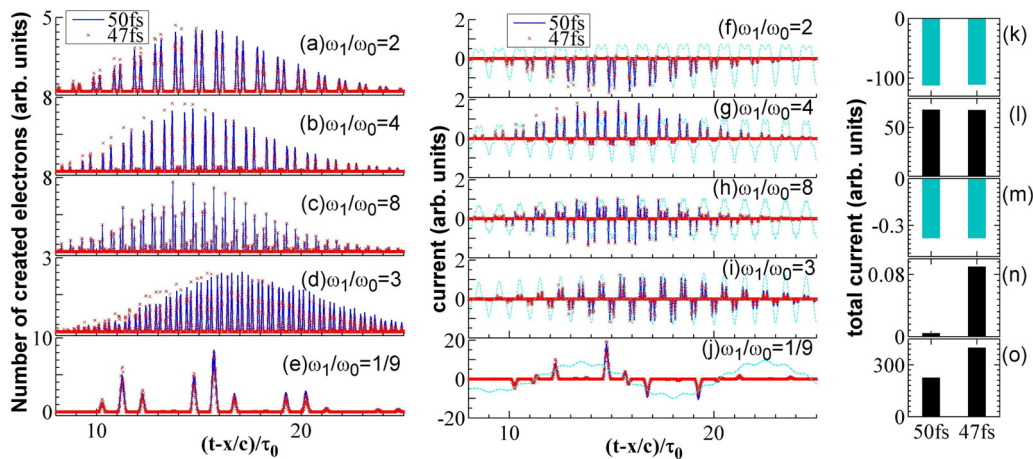


FIG. 3. (a)–(e) Number distribution of electrons as a function of laser-pulse envelope position ($t - x/c$), where the pulse front is at $t - x/c = 0$ and the electrons are created via ionization by the two-color laser pulses with different frequency ratios in different plots. The two curves in each plot correspond to laser durations of 50 fs and 47 fs, respectively. (f)–(j) The corresponding currents $-J$ ($J = -en_e v$) formed due to the ionization, where in each plot the cyan dash line shows the normalized velocities v or the normalized vector potentials $-A$ of the 50 fs two-color laser pulses. (k)–(o) The corresponding total currents after the passage of the two-color laser pulses with durations 50 fs and 47 fs, where the colors of the bars display the current signs.

the current generation is periodic and its period is $b\tau_0$ or $a\tau_1$, where $\omega_1/\omega_0 = a : b$. In the case with $\omega_1/\omega_0 = 2$, the currents formed in each ionization points have the same sign [17,36], as seen in Fig. 3(f). In the case with $\omega_1/\omega_0 = 1/9$, the currents formed at the first three points and within the first half ω_1 -laser cycle (starting around $10\tau_0$) have the signs opposite to the ones within the followed half ω_1 -laser cycle (starting around $15\tau_0$), as observed in Fig. 3(j). According to simple analysis as done in Ref. [36], the currents formed within the first half ω_1 -laser cycle should be completely counteracted by the ones within the other half ω_1 -laser cycle and THz radiation should not be generated if the laser pulses have sufficiently large number of cycles [this is the case with $\omega_1/\omega_0 = 3$ shown in Figs. 3(d), 3(i) and 3(n)]. However, in our case the laser duration is 50 fs and the laser intensity at the first half ω_1 -laser cycle is significantly different from that at the other half ω_1 -laser cycle, since the displacement between them is 12 fs. Hence the respective currents formed within the two half cycles cannot completely counteract each other, as observed in Fig. 3(j). This causes the total net current to be even stronger than the case with $\omega_1/\omega_0 = 2$ [see Figs. 3(o) and 3(k)] and consequently the THz radiation is more powerful (see Fig. 1). In the same way, one can explain the powerful THz generation at other low ω_1/ω_0 , e.g., 1/7, 3/10, 1/5, etc.

The net currents and the THz radiation are formed in the case with the lower ω_1/ω_0 due to a larger period $b\tau_0$ or $a\tau_1$ of the two linear-superposition laser fields and resulting asymmetry of the laser intensity in the positive and negative half period. Therefore, periodic laser fields are not necessary for the THz generation in this case. For example, we take $\omega_1/\omega_0 = 0.112$ ($a = 112$ and $b = 1000$) in our simulation and a strong radiation can be generated. One can consider the total laser fields of the 50 fs pulses not to be periodic since $b\tau_0 = a\tau_1 \gg 50$ fs. In this case the current and the radiation strength strongly depend on the laser duration, as in the case with $\omega_1/\omega_0 = 1/9$ [see Fig. 3(o)]. This is different from the case with the higher ω_1/ω_0 [e.g., see Figs. 3(f)–3(h) with $\omega_1/\omega_0 = 2, 4, 8$], where the current formation is slightly affected by the change of the laser duration [see Figs. 3(k)–3(m)]. For example, in Figs. 3(a) and 3(e), when we decrease the laser duration from 50 fs to 47 fs, more electrons are created at a smaller $t - x/c$ and less at a larger $t - x/c$ (at $t - x/c > 15\tau_0$) because the laser intensity peak is shifted forwards. In the case with $\omega_1/\omega_0 = 2$, the total current is nearly not changed [see Fig. 3(k)] since the decrease of the currents at larger $t - x/c$ can be compensated by the increase of the currents at smaller $t - x/c$ [see Fig. 3(f)]. This is not the case with $\omega_1/\omega_0 = 1/9$. Compared with the case with the 50 fs duration, in the case with the 47 fs duration the positive currents at about $t - x/c = 12\tau_0$ and $15\tau_0$ are increased and the negative currents at about $t - x/c = 17\tau_0$ and $19\tau_0$ are decreased [see Fig. 3(j)] and therefore the total positive current is increased [see Fig. 3(o)].

A. Three series of ω_1/ω_0 for high-efficiency and stable THz generation

From Figs. 1(a) and 1(b) one can also observe that when the laser duration is changed, three series $\omega_1/\omega_0 = 2n$, $n + 1/2$, and $n \pm 1/3$ (n is a positive integer) show better stability in the

THz strengths than the cases with lower ω_1/ω_0 , although in which strong THz radiation can be generated. In the three series, the periodic current generation has a small period determined by $b\tau_0$ (it is τ_0 , $2\tau_0$, and $3\tau_0$ for the series $2n$, $n + 1/2$, and $n \pm 1/3$, respectively) and the net currents generated in different periods have the same signs (they could be generated in a few ionization points in each period), as seen in Figs. 3(f)–3(h). A small change of the laser duration (from 50 fs to 47 fs and 40 fs in our simulations) slightly affects the ionization region or the ionization point number and the electron number in each ionization point, as shown in Fig. 3. Therefore, the THz strengths hardly change with the varying laser duration.

In Fig. 2 we increase the laser intensity from $I_0 = I_1 = 10^{14}$ W/cm² to 4×10^{14} W/cm², which causes the THz strengths to be slightly changed for the $2n$ and $n + 1/2$ series, but they are significantly changed for the $n \pm 1/3$ series. This can be explained as follows. When the intensity is increased, the ionization points shift away from the intensity peak to the pulse leading edge and the ionization region as well as the ionization point number are reduced, which was demonstrated in Refs. [19,36]. The series $n \pm 1/3$ have a longer period $b\tau_0$ ($b = 3$) of the periodic current generation than the other two series and, therefore, the reduction of the ionization point number affects the net current and THz generation more significantly. For the same reason, the series $\omega_1/\omega_0 = 2n$ with the shortest period τ_0 should have the best stability against the change of the laser intensity.

On the other hand, if the duration is significantly decreased, which causes a significant decrease of the ionization point number, the stability of the series $\omega_1/\omega_0 = 2n$ can become worse. This can be seen from the PIC simulation results in Ref. [19]: with a 12 fs laser duration, the THz strength shows oscillatory dependence on the laser intensity. By contrast, one can see in Fig. 5 that with the 50 fs laser duration, the THz strength shows saturation as the laser intensity is increased, i.e., the strength is stable with the increasing laser intensity.

From Fig. 2 one can also see that the THz strengths tend to decrease with the growth of n in the three series and the strengths are close to zero with a sufficiently large n . With the same n , the $2n$ series have the highest efficiency of THz generation, e.g., one can compare the THz strengths with $\omega_1/\omega_0 = 2$, $3/2$, and $2/3$. These results can be explained in the following by a model based on gas ionization by two linear-superposition laser fields and subsequent net current or velocity gain. Note that we classify $\omega_1/\omega_0 = 1/4$ and $1/2$ into $2n$ series. We will show that the analysis to $\omega_1/\omega_0 = 4$ and 2 can be directly applied to $\omega_1/\omega_0 = 1/4$ and $1/2$ by a linear scaling law of the laser wavelength derived below.

B. Model and a wavelength scaling law

The following analysis is based on net or transient current formation and THz generation via asymmetric ionization of tunneling in two linear-superposition laser fields. The idea was proposed by Kim *et al.* in 2007 [17] and verified by experiments [17,18]. Then, it was well established with near-field radiation generation due to the current dynamics in plasma [19,36,42] and far-field radiation obtained by a (3+1)-dimensional simulation approach including a comprehensive

description of the propagation of lasers and radiation [40,41]. Here, we apply the near-field radiation model, since the observed far-field radiation is expected to be composed of near-field radiation sources [27,41]. Based on the net current formation due to ionization [17], Wang *et al.* [19] proposed a model including the net current dynamics due to plasma response, which causes the radiation with a frequency at the plasma oscillation frequency; then a solution of the radiation emitted from a plasma was given in a one-dimensional approximation or a plane wave approximation [42]; recently, this model has been extended to the case with an external magnetic field imposed [31].

We take the electric fields of the two laser pulses as $\mathbf{E} = \vec{e}_y [a_0 \sin(\omega_0 \psi) + a_1 \sin(\omega_1 \psi)] f(\psi)$, where $\psi = t - x/c$ and $f(\psi)$ is the envelope profile of the laser pulses. We consider the laser duration around 50 fs and thus $\partial f(\psi)/\partial \psi \ll \omega_0$ and ω_1 in the case $n \geq 1$. Then the vector potential can be given by $\mathbf{A} = \vec{e}_y \frac{c}{\omega_0} [a_0 \cos(\omega_0 \psi) + \frac{\omega_0}{\omega_1} a_1 \cos(\omega_1 \psi)] f(\psi)$. According to Refs. [36], when an electron is born due to ionization, it will gain a net transverse velocity $\mathbf{v} = -e\mathbf{A}(\psi^0)/m_e c$ after the passage of the laser pulses, where ψ^0 is the born position of the electron. Generally ψ^0 is around an extremum of E , at which the ionization occurs with the highest probability. An extremum of E appears when $\partial E/\partial \psi = 0$, i.e.,

$$a_0 \cos(\omega_0 \psi^0) = -\frac{a_1 \omega_1}{\omega_0} \cos(\omega_1 \psi^0). \quad (1)$$

Then, the electron created at ψ^0 gains the net velocity as

$$v = \frac{ea_0}{m_e \omega_0} \cos(\omega_0 \psi^0) f(\psi^0) \left[\frac{\omega_0^2}{\omega_1^2} - 1 \right]. \quad (2)$$

According to Eqs. (1) and (2), one can derive a scaling law of the laser wavelength under the following conditions. We fix the ratio ω_1/ω_0 and the laser field strengths a_0 and a_1

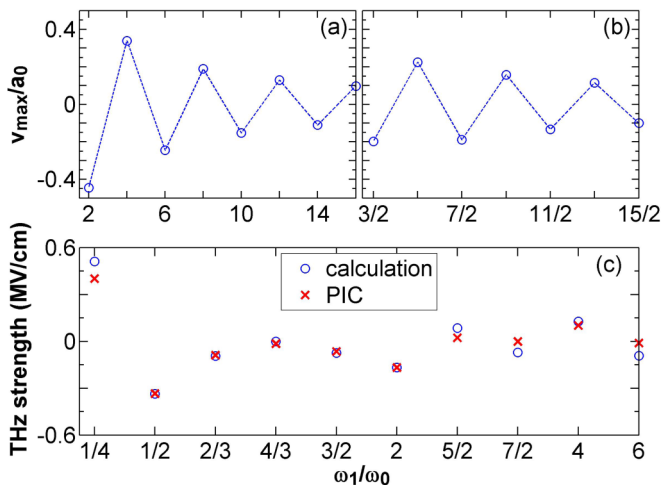


FIG. 4. (a),(b) Velocities v (normalized by $ea_0/m_e \omega_0$) of the electrons created in the strongest ionization points, calculated according to Eq. (2), where the frequency ratios are taken as $2n$ and $n + 1/2$ in (a) and (b), respectively. (c) The THz field strength as a function of the laser frequency ratio, where the red stars show PIC results and the blue circles show calculation results. The calculation results are fitted through E_{THz}/v at $\omega_1/\omega_0 = 2$ [$E_{THz}(\omega_1/\omega_0 = 2)$ is obtained from our PIC result and $v(\omega_1/\omega_0 = 2)$ from Eq. (2)].

(note that a_0 can be different from a_1). Equation (1) gives $\cos(\omega_0 \psi^0) = \alpha \cos(\omega_1 \psi^0)$, and α is not varied with the change of ω_0 , and then ψ^0 is not changed either. If the laser duration is much longer than both the laser cycles τ_0 and τ_1 , $f(\psi^0)$ will nearly not change with ω_0 . Hence properties of the net velocity generation are kept unchanged if one varies ω_0 and fixes ω_1/ω_0 . Then, one can obtain

$$v \propto \frac{1}{\omega_0} \propto \lambda_0. \quad (3)$$

According to the results given in Refs. [19,31,42], the THz strength E_{THz} is linearly proportional to the net velocity and therefore the wavelength scaling law for the THz strength can be written by

$$E_{THz} \propto \lambda_0. \quad (4)$$

Note that Eqs. (3) and (4) hold only when the ionization rates do not depend on the laser wavelength. In this study, we take $I_0 = I_1 \geq 10^{14}$ W/cm², the Keldysh parameter [43] γ_K for hydrogen is less than 1, and therefore the ionization is in the tunneling regime [43,44]. In this regime, the ionization rates are independent of the wavelength [45,46]. When the laser intensity is sufficiently low (or the intensity is depleted due to a long distance propagation [35]), the ionization will enter the multiphoton regime and it will have complex dependence on the wavelength. In this case, the linear scaling of the net current and THz strength with the wavelength is broken, as shown in Refs. [34,35].

Equation (1) gives multiple solutions to ψ^0 and these solutions in the first half period of the total laser field are symmetric to those in the other half period, where a period of the laser field is τ_0 , $2\tau_0$, and $3\tau_0$, respectively, for the series $\omega_1/\omega_0 = 2n$, $n + 1/2$, and $n \pm 1/3$. Since the solutions are difficult to derive analytically, we numerically solve Eqs. (1) and (2) and present the results in Table I. In this table we list the net velocities of the electrons created in the first, second, and third strongest ionization points, where the strongest

TABLE I. Velocities v (normalized by $ea_0/m_e \omega_0$) of the electrons created in different ionization points in a half period of the total laser fields and around the laser pulse peak. Note that the same velocity values appear symmetrically in the other half period. The laser frequency ratio is given in the first column and the following columns show the velocities gained from the first, second, and third strongest ionization points determined according to our PIC simulation results, which are partially shown in Figs. 3(f)–3(j). Here, the strongest ionization points mean the ones where the most electrons are created.

| | 1st | 2nd | 3rd |
|---------------------------|-------|-------|-------|
| $\omega_1/\omega_0 = 1/4$ | 1.36 | -3.38 | |
| $\omega_1/\omega_0 = 1/2$ | -0.89 | | |
| $\omega_1/\omega_0 = 2$ | -0.44 | | |
| $\omega_1/\omega_0 = 4$ | 0.34 | -0.87 | |
| $\omega_1/\omega_0 = 6$ | -0.25 | 0.67 | |
| $\omega_1/\omega_0 = 8$ | 0.19 | -0.54 | 0.88 |
| $\omega_1/\omega_0 = 3/2$ | -0.20 | 0.50 | |
| $\omega_1/\omega_0 = 5/2$ | 0.23 | -0.62 | |
| $\omega_1/\omega_0 = 2/3$ | -0.30 | 0.77 | |
| $\omega_1/\omega_0 = 4/3$ | -0.18 | 0.30 | -0.43 |

ionization points mean the ones with the most electrons created. These points are confirmed according to the laser electric-field values and our PIC simulation results [partially shown in Figs. 3(f)–3(j)]. Furthermore, we display the net velocities in the strongest ionization points in Figs. 4(a) and 4(b) for the series $\omega_1/\omega_0 = 2n$ and $n + 1/2$, respectively. The velocities tend to decrease with the increasing n and their signs are changed as n grows by 1, which is in agreement with the simulation results given in Fig. 2. One can also see in Table I that, with the same n , the $2n$ series have higher velocities in the strongest ionization points than the other two series, which is in agreement with our PIC simulation shown in Fig. 2.

One can notice that the decrease of the THz strength with n in Fig. 2 is more significant than in Figs. 4(a) and 4(b). This is because the velocities in the second strongest ionization points [see Table I] have the opposite signs and larger absolute values than the ones in the strongest points (see Table I). Then, the net currents in the strongest points are counteracted [see Figs. 3(g) and 3(h)]. With a larger n , e.g., Fig. 3(h), the number of the created electrons in the second (and even the third) strongest point is comparable with the number in the strongest point because the displacement between the two points becomes smaller and the laser fields in these points have a smaller difference. Then, the current in the strongest ionization point can be nearly completely counteracted, which causes the total current to be weak [see Fig. 3(m)] and consequently the THz generation is ineffective with a large n .

In Fig. 4(c) we compare the PIC results with the calculation results of Eq. (2), where we only use the electron velocity in the strongest ionization point. The two results agree with each other for small n since nearly all electrons are created in the strongest ionization point, e.g., $\omega_1/\omega_0 = 1/2, 2, 2/3$, and $3/2$. There appear considerable differences when n becomes large, e.g., $\omega_1/\omega_0 = 6$ and $7/2$, with which many electrons can be created in the second and third strongest ionization points.

In particular, the results in Fig. 4(c) show good agreement with the linear wavelength scaling law for the THz strength given by Eqs. (3) and (4). One can see the THz strength ratio is 2:1 between the cases $\omega_1/\omega_0 = 1/2$ and $\omega_1/\omega_0 = 2$, the strength ratio is 3:2 between $\omega_1/\omega_0 = 2/3$ and $\omega_1/\omega_0 = 3/2$, and the strength ratio is 4:1 between $\omega_1/\omega_0 = 1/4$ and $\omega_1/\omega_0 = 4$. Here we take $I_1 = I_0$ in our simulations (following Ref. [37]) and then can apply Eq. (4) with interchanging the indices 0 and 1 in the frequencies. For example, with $\omega_1/\omega_0 = 2$ the laser wavelengths λ_1 and λ_0 are $0.4 \mu\text{m}$ and $0.8 \mu\text{m}$, respectively; with $\omega_1/\omega_0 = 1/2$ the laser wavelengths λ_1 and λ_0 are $1.6 \mu\text{m}$ and $0.8 \mu\text{m}$, respectively. With a given frequency ratio $2/1$, the $1.6 \mu\text{m}$ laser is the fundamental one in the latter case, while in the former case the $0.8 \mu\text{m}$ laser is the fundamental one. Therefore, as the fundamental wavelength is changed by a factor of 2, the THz strength should change by the same factor according to the wavelength scaling law.

If I_0 and I_1 are different, the linear wavelength scaling is still valid with a fixed frequency ratio, since the tunneling ionization rates depend on the total laser intensity and does not depend on the wavelength. In Fig. 5, we show the PIC simulation results with $I_1 = 0.25I_0$ and one can see the linear scaling holds well. Note that the scaling law $E_{\text{THz}} \propto \lambda_0$ or $\varepsilon_{\text{THz}} \propto \lambda_0^2$ (ε_{THz} is the THz energy) disagrees with the scaling law $\varepsilon_{\text{THz}} \propto \lambda_0^{4.6}$ found in experiments [34]. There are two

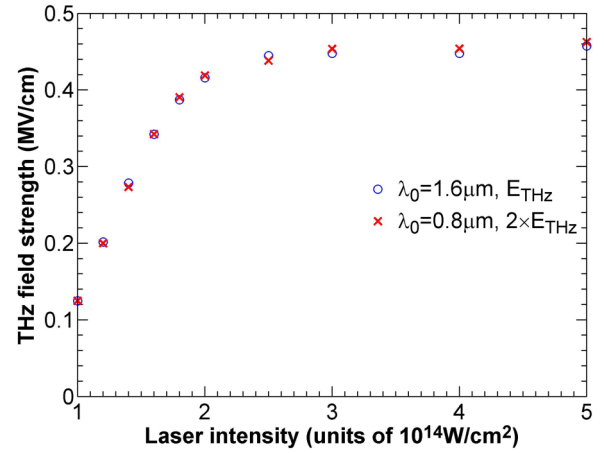


FIG. 5. THz field strength as a function of the ω_0 -laser intensity I_0 , where in the PIC simulations we fix $\omega_1/\omega_0 = 2$ and $I_1/I_0 = 0.25$. We perform two groups of simulations with different ω_0 -laser wavelengths of $1.6 \mu\text{m}$ and $0.8 \mu\text{m}$ shown by the blue circles and the red crosses, respectively, where the THz strengths are multiplied by a factor of 2 in the case with the wavelength of $0.8 \mu\text{m}$.

reasons at least. First, we fix the laser intensity, duration, and spot size as the wavelength is varied. In Ref. [34] the laser energy was fixed with the varying wavelength, which results in the change of the laser intensity and laser-gas or laser-plasma interaction volume. Second, our scaling law is given in the tunneling ionization regime in which the ionization rates do not depend on the wavelength. In Ref. [34] the ionization could stride across the tunneling regime and the multiphoton ionization regime as the laser wavelength and intensity is changed. In the multiphoton regime, the ionization rates depend on the wavelength. The two factors above cause a stronger dependence of the THz energy on the wavelength.

IV. SUMMARY

In summary, we have investigated THz generation via the two-color laser scheme with the frequency ratio ω_1/ω_0 in the nearly whole range possibly adopted in laboratories currently. For a conventional $0.8 \mu\text{m}$ and 50fs laser pulse (the ω_0 pulse), THz radiation may be generated at any ω_1/ω_0 when $\omega_1/\omega_0 < 1/3$. Even at $\omega_1/\omega_0 = a/b = 1/5, 1/7$ with an even $a + b$, the radiation can be generated and its strength could be higher than the one at $\omega_1/\omega_0 = 2$, the original two-color scheme. In the case with the low ω_1/ω_0 , the net current is formed due to the asymmetry of the laser intensity in the positive and negative half period of the laser fields. Therefore, the THz strength is sensitive to the laser pulse duration and periodic laser fields are not necessary for the THz generation.

With $\omega_1/\omega_0 > 1/3$, there are three series with $\omega_1/\omega_0 = 2n, n + 1/2, n \pm 1/3$ for high-efficiency and stable THz generation, where periodic laser fields are necessary to ensure that net currents formed in different periods have the same sign. Among them, the $2n$ series shows the highest efficiency and the best stability against the change of the laser duration and intensity. For the three series the THz strength basically decreases with the increasing n . The strength scales linearly

with the laser wavelength, which holds in the tunneling ionization regime.

ACKNOWLEDGMENTS

This work was supported by the National Basic Research Program of China (Grants No. 2013CBA01500 and No. 2014CB339801), the National Natural Science Foundation of China (Grants No. 11375261, No. 11775302, No. 11421064,

No. 11374210, No. 113111048, and No. 11520101003), Science Challenge Project of China (Grant No. TZ2016005), and the Strategic Priority Research Program of the Chinese Academy of Sciences (Grants No. XDB16010200 and No. XDB07030300). Z.M.S. acknowledges the support of a Leverhulme Trust Research Grant at the University of Strathclyde, EC's Horizon 2020 EuPRAXIA (Grant No. 653782), and UK Engineering and Physical Sciences Research Council (Grant No. EP/N028694/1).

-
- [1] D. Grischkowsky, S. Keiding, M. Exter, and Ch. Fattinger, *J. Opt. Soc. Am. B* **7**, 2006 (1990).
- [2] J. C. Cao, *Phys. Rev. Lett.* **91**, 237401 (2003).
- [3] M. Jewariya, M. Nagai, and K. Tanaka, *Phys. Rev. Lett.* **105**, 203003 (2010).
- [4] T. Kampfrath, K. Tanaka, and K. Nelson, *Nat. Photon.* **7**, 680 (2013).
- [5] B. Alexandrov, M. Phipps, L. Alexandrov, L. Booshehri, A. Erat, J. Zabolotny, C. Mielke, H.-T. Chen, G. Rodriguez, K. Rasmussen, J. S. Martinez, A. R. Bishop, and A. Usheva, *Sci. Rep.* **3**, 1184 (2013).
- [6] R. Woodward, V. Wallace, R. Pye, B. Cole, D. Arnone, E. Linfield, and M. Pepper, *J. Invest. Dermatol.* **120**, 72 (2003).
- [7] Y. T. Li, C. Li, M. L. Zhou, W. M. Wang, F. Du, W. J. Ding, X. X. Lin, F. Liu, Z. M. Sheng, X. Y. Peng *et al.*, *Appl. Phys. Lett.* **100**, 254101 (2012).
- [8] A. Gopal, S. Herzer, A. Schmidt, P. Singh, A. Reinhard, W. Ziegler, D. Brömmel, A. Karmakar, P. Gibbon, U. Dillner *et al.*, *Phys. Rev. Lett.* **111**, 074802 (2013).
- [9] G. Q. Liao, Y. T. Li, C. Li, L. N. Su, Y. Zheng, M. Liu, W. M. Wang, Z. D. Hu, W. C. Yan, J. Dunn, J. Nilsen, J. Hunter, Y. Liu, X. Wang, L. M. Chen, J. L. Ma, X. Lu, Z. Jin, R. Kodama, Z. M. Sheng, and J. Zhang, *Phys. Rev. Lett.* **114**, 255001 (2015).
- [10] G.-Q. Liao, Y.-T. Li, Y.-H. Zhang, H. Liu, X.-L. Ge, S. Yang, W.-Q. Wei, X.-H. Yuan, Y.-Q. Deng, B.-J. Zhu, Z. Zhang, W.-M. Wang, Z.-M. Sheng, L.-M. Chen, X. Lu, J.-L. Ma, X. Wang, and J. Zhang, *Phys. Rev. Lett.* **116**, 205003 (2016).
- [11] W. J. Ding and Z. M. Sheng, *Phys. Rev. E* **93**, 063204 (2016).
- [12] Z. Jin, H. B. Zhuo, T. Nakazawa, J. H. Shin, S. Wakamatsu, N. Yugami, T. Hosokai, D. B. Zou, M. Y. Yu, Z. M. Sheng, and R. Kodama, *Phys. Rev. E* **94**, 033206 (2016).
- [13] D. J. Cook and R. M. Hochstrasser, *Opt. Lett.* **25**, 1210 (2000).
- [14] M. Kress, T. Löffler, S. Eden, M. Thomson, and H. G. Roskos, *Opt. Lett.* **29**, 1120 (2004).
- [15] T. Bartel, P. Gaal, K. Reimann, M. Woerner, and T. Elsaesser, *Opt. Lett.* **30**, 2805 (2005).
- [16] X. Xie, J. Dai, and X.-C. Zhang, *Phys. Rev. Lett.* **96**, 075005 (2006).
- [17] K. Y. Kim, J. H. Glowonia, A. J. Taylor, and G. Rodriguez, *Opt. Express* **15**, 4577 (2007).
- [18] K. Y. Kim, A. J. Taylor, J. H. Glowonia, and G. Rodriguez, *Nat. Photon.* **2**, 605 (2008).
- [19] W.-M. Wang, Z.-M. Sheng, H.-C. Wu, M. Chen, C. Li, J. Zhang, and K. Mima, *Opt. Express* **16**, 16999 (2008).
- [20] X.-Y. Peng, C. Li, M. Chen, T. Toncian, R. Jung, O. Willi, Y.-T. Li, W.-M. Wang, S.-J. Wang, F. Liu, A. Pukhov, Z.-M. Sheng, and J. Zhang, *Appl. Phys. Lett.* **94**, 101502 (2009).
- [21] T.-J. Wang, Y. Chen, C. Marceau, F. Théberge, M. Châteauneuf, J. Dubois, and S. L. Chin, *Appl. Phys. Lett.* **95**, 131108 (2009).
- [22] Y. Chen, T.-J. Wang, C. Marceau, F. Théberge, M. Châteauneuf, J. Dubois, O. Kosareva, and S. L. Chin, *Appl. Phys. Lett.* **95**, 101101 (2009).
- [23] W.-M. Wang, P. Gibbon, Z.-M. Sheng, and Y.-T. Li, *Phys. Rev. A* **90**, 023808 (2014).
- [24] A. Debayle, P. González de Alaiza Martínez, L. Gremillet, and L. Bergé, *Phys. Rev. A* **91**, 041801(R) (2015).
- [25] P. González de Alaiza Martínez, X. Davoine, A. Debayle, L. Gremillet, and L. Bergé, *Sci. Rep.* **6**, 26743 (2016).
- [26] V. A. Andreeva, O. G. Kosareva, N. A. Panov, D. E. Shipilo, P. M. Solyankin, M. N. Esaulkov, P. González de Alaiza Martínez, A. P. Shkurinov, V. A. Makarov, L. Bergé, and S. L. Chin, *Phys. Rev. Lett.* **116**, 063902 (2016).
- [27] Z. Zhang, Y. Chen, M. Chen, Z. Zhang, J. Yu, Z. Sheng, and J. Zhang, *Phys. Rev. Lett.* **117**, 243901 (2016).
- [28] H.-C. Wu, J. Meyer-ter-Vehn, and Z.-M. Sheng, *New J. Phys.* **10**, 043001 (2008).
- [29] J. Dai, N. Karpowicz, and X.-C. Zhang, *Phys. Rev. Lett.* **103**, 023001 (2009).
- [30] H. Wen and A. M. Lindenberg, *Phys. Rev. Lett.* **103**, 023902 (2009).
- [31] W.-M. Wang, P. Gibbon, Z.-M. Sheng, and Y.-T. Li, *Phys. Rev. Lett.* **114**, 253901 (2015).
- [32] W.-M. Wang, S. Kawata, Z.-M. Sheng, Y.-T. Li, J. Zhang, L. M. Chen, L. J. Qian, and J. Zhang, *Opt. Lett.* **36**, 2608 (2011).
- [33] Y. Bai, L. Song, R. Xu, C. Li, P. Liu, Z. Zeng, Z. Zhang, H. Lu, R. Li, and Z. Xu, *Phys. Rev. Lett.* **108**, 255004 (2012).
- [34] M. Clerici, M. Peccianti, B. E. Schmidt, L. Caspani, M. Shalaby, M. Giguère, A. Lotti, A. Couairon, F. Légaré, T. Ozaki, D. Faccio, and R. Morandotti, *Phys. Rev. Lett.* **110**, 253901 (2013).
- [35] L. Bergé, S. Skupin, C. Köhler, I. Babushkin, and J. Herrmann, *Phys. Rev. Lett.* **110**, 073901 (2013).
- [36] W.-M. Wang, Y.-T. Li, Z.-M. Sheng, X. Lu, and J. Zhang, *Phys. Rev. E* **87**, 033108 (2013).
- [37] V. A. Kostin, I. D. Laryushin, A. A. Silaev, and N. V. Vvedenskii, *Phys. Rev. Lett.* **117**, 035003 (2016).
- [38] P. González de Alaiza Martínez, I. Babushkin, L. Bergé, S. Skupin, E. Cabrera-Granado, C. Köhler, U. Morgner, A. Husakou, and J. Herrmann, *Phys. Rev. Lett.* **114**, 183901 (2015).
- [39] W.-M. Wang, P. Gibbon, Z.-M. Sheng, and Y.-T. Li, *Phys. Rev. E* **91**, 013101 (2015).
- [40] I. Babushkin, W. Kuehn, C. Köhler, S. Skupin, L. Bergé, K. Reimann, M. Woerner, J. Herrmann, and T. Elsaesser, *Phys. Rev. Lett.* **105**, 053903 (2010).

- [41] I. Babushkin, S. Skupin, A. Husakou, C. Köhler, E. Cabrera-Granado, L. Bergé, and J. Herrmann, [New J. Phys.](#) **13**, 123029 (2011).
- [42] W.-M. Wang, S. Kawata, Z.-M. Sheng, Y.-T. Li, and J. Zhang, [Phys. Plasmas](#) **18**, 073108 (2011).
- [43] L. V Keldysh, *Sov. Phys. JETP* **20**, 1307 (1965).
- [44] G. Gibson, T. S. Luk, and C. K. Rhodes, [Phys. Rev. A](#) **41**, 5049 (1990).
- [45] M. V. Ammosov, N. B. Delone, and V. P. Krainov, *Sov. Phys. JETP* **64**, 1191 (1986).
- [46] B. M. Penetrante and J. N. Bardsley, [Phys. Rev. A](#) **43**, 3100 (1991).